SSC19-WKV-09

AERO & VISTA: Demonstrating HF Radio Interferometry with Vector Sensors

Frank D. Lind, Philip J. Erickson, Michael Hecht, Mary Knapp, Geoffrey Crew, Ryan Volz, John Swoboda
MIT Haystack Observatory
99 Millstone Rd. Westford, MA 01886; 617-715-5561
flind@mit.edu

Frank Robey, Mark Silver, Alan J. Fenn
MIT Lincoln Laboratory
244 Wood St, Lexington MA 02421; 781-981-9582
robey@ll.mit.edu

Benjamin Malphrus
Morehead State University
150 University Blvd, Morehead, KY 40351; 606-783-2212
[Second Author Email]

Kerri Cahoy
Massachusetts Institute of Technology
77 Massachusetts Ave. Cambridge, MA 02139; 650-324-6005
kcahoy@mit.edu

ABSTRACT

AERO (Auroral Emission Radio Observer) and VISTA (Vector Interferometry Space Technology using AERO) are recently selected NASA HTIDeS CubeSat missions for terrestrial auroral science and radio interferometric technology demonstration. The AERO and VISTA CubeSats both host vector sensing antenna systems providing advanced electromagnetic capabilities. Together, they will provide the first in-space demonstration of interferometric imaging, beamforming, and nulling using electromagnetic vector sensors at low frequencies (100 kHz – 15 MHz). A key goal of the joint missions' technology demonstration is to validate theoretical sensor performance modeling indicating that interferometric arrays composed of vector sensors will be able to maintain sensitivity even in the presence of terrestrial interference. If validated in flight, this capability would relax the requirement that space-based low frequency interferometers be placed far from the Earth (e.g. lunar orbit), and the closer communications range will significantly increase the data volume returned from space-based radio telescope systems. The two-spacecraft AERO+VISTA mission will address the auroral science goals of AERO (Erickson et al. 2018, SSC18) while adding three additional technology demonstration goals enabled by the second CubeSat, VISTA.

AERO's science objectives are:
1) Characterize auroral radio emissions in the ionosphere;
2) Connect radio emissions to overall auroral geospace system; and
3) Demonstrate polarimetric HF radio detection with a vector sensor.

VISTA's objectives, achieved in concert with AERO, are:
1) Validate algorithms for, and sensitivity advantages of, vector sensor interferometry;
2) Apply vector sensor interferometry to auroral radio emissions; and
3) Perform a survey of the low frequency RFI environment in low Earth orbit to assess the suitability of the environment for future multi-element interferometric constellations.

The AERO and VISTA CubeSats will launch and deploy together into a polar orbit. Once in orbit, the relative separation between the spacecraft will be controlled via differential drag in order to perform the vector sensor interferometry demonstration. After this demonstration is complete, the spacecraft will be allowed to drift apart. Throughout the mission, AERO will carry out science activities focused on observing and localizing natural auroral

radio emission while VISTA will perform its RFI survey. At times of high auroral activity, both AERO and VISTA will shift to data collection over the auroral zones, providing new insight into the time evolution of auroral emission features. In this paper, we will present simulation results for vector sensor interferometry as compared to traditional interferometry between crossed dipole or tripole antennas. Launch for AERO and VISTA is planned for 2021.

INTRODUCTION

Space radio interferometry is a critical technology for advancing scientific investigation of radio emission from the solar corona, inner heliosphere, auroral radio emissions from Earth, and radio emissions from other planetary bodies in the solar system. Future constellations of satellites will be required if we are to achieve sufficient sensitivity, angular resolution, and measurement speed for these scientific objectives.

The NASA H-TIDES-funded AERO mission will flight qualify a vector sensor (VS), a novel device that measures the full electric and magnetic field vector at a single point in space, to accomplish four auroral science goals [1]. VISTA and AERO, twin CubeSats sharing a common design and capabilities, will expand the impact of the VS by demonstrating *vector sensor interferometry* (VSI) through executing beamforming and nulling. This technology will serve as a pathfinder for radio constellations of CubeSats yielding the same sensitivity as missions that employ more than twice as many dipole or tripole antennas [2] for flights in a radio quiet environment such as the lunar far side.

The VS can also localize and null strong sources of RF interference, allowing low frequency VSI constellations to be deployed near Earth despite terrestrial interference. Compared to conventional low dimensional sensor platforms, these capabilities result in less costly missions, reduced risk, and significantly higher data volume returned to Earth. One application of importance is spot mapping of solar radio burst emissions, as detection and tracking of these features can contribute to the prediction of space weather [3]. More broadly, VSI is a stepping-stone to a novel remote sensing platform with applicability to broad classes of plasma waves and radiation in the heliosphere.

Radio emissions from auroral structures in the near-Earth space environment reflect the inherent complexity of the auroral ionospheric plasma conditions and processes. VISTA will extend the scientific reach of the AERO auroral investigation. In addition to providing vastly more data, improving spatial and temporal coverage, and mitigating risk, VISTA will enhance AERO by enabling imaging of complex auroral emission regions and boundaries with high spatial and temporal resolution. For selected events, this will include imaging of radio emission structures and measurement of short time scale dynamics by offering a short revisit time for the same spatial region.

VISTA MISSION GOALS

VISTA has three goals:

1. Validate the advantages of VSI in space using ground-based radio beacons by:
    - Comparing measurements derived from sub-elements of the vector sensor (dipole and crossed-dipole) with those derived from the full vector sensor.
    - Demonstrating beamforming, localization, and nulling of the ground-based radio beacon signals as representative of ‘interference’ mitigation methods.
    - Quantifying improvements in angular resolution, variance, and tolerance to interference.
2. Apply VSI to auroral radio emissions by:
    - Demonstrating interferometry and imaging of AKR radio signals in the presence of real-world noise and interference.
    - Quantifying the performance improvements of VSI relative to a single VS.
    - Investigating imaging algorithms and approaches to enhance the measurement of auroral kilometric radiation (AKR).
3. Characterize the types, levels, spatial and polarization characteristics, and sources of low and medium frequency RFI in low Earth orbit by:
    - Periodically sampling the environment over the course of VISTA orbits.
    - Providing full spectral coverage of observed sources (0.1 to 15 MHz) with angle and polarization knowledge.
    - Measuring RFI from AERO and demonstrating beamforming and nulling of AERO-to-VISTA interference above 5 MHz (i.e. the AERO/VISTA design effectively eliminates RFI in the critical science frequency window *below* 5 MHz).

VISTA TECHNOLOGY

Vector sensor interferometry (VSI) is a stepping-stone to a novel remote sensing platform with direct applicability to broad classes of plasma waves and radiation in the heliosphere.

Vector Sensor Interferometry (VSI)

A VS samples the amplitude and phase of the electric (E) and magnetic (H) field at a single location in space and with a common phase center. To do this, a vector sensor is composed of three orthogonal dipole elements and three orthogonal loop elements. The vector sensor is named for its capacity to fully measure the electromagnetic vector field rather than the scalar measurements associated with an antenna that does not fully measure both E and H. Consequences of sensing the full E and H vectors are that the vector sensor natively measures full polarization information and the Poynting vector of an electromagnetic wave.

Consider the electromagnetic field in space, characterized by the electric and magnetic fields in three spatial dimensions for a particular source, p,

$$\boldsymbol{\mathcal{F}}(p) = \begin{bmatrix} E_x(p) \\ E_y(p) \\ E_z(p) \\ H_x(p) \\ H_y(p) \\ H_z(p) \end{bmatrix} \quad (1)$$

Maxwell's Equations describe the relationship between the electric and magnetic fields. For free space Faraday's law, $\nabla \times \boldsymbol{E} = -\frac{\partial \mathbf{B}}{\partial t}$ and Ampère's law, $\nabla \times \boldsymbol{B} = \mu_0 \varepsilon_0 \frac{\partial \mathbf{E}}{\partial t}$ lead to the well-known definition of the Poynting, or source direction, vector $\mathbf{S} = \mathbf{E} \times \mathbf{H}$, and the relationship between the time-averaged intensity of the electric and magnetic field, $|\mathbf{H}| = \sqrt{\frac{\varepsilon_0}{\mu_0}}|\boldsymbol{E}|$. In free space, $\boldsymbol{B} = \mu_o \mathbf{H}$. Measurement of both E and H with a common phase center provides information about both the Poynting vector and the correlations between the field components.

In addition to their single-element directional remote sensing capabilities, VS elements can be used in sparse arrays to perform interferometric observations and fully polarimetric synthesis imaging [4], [5]. In combination with an appropriate image deconvolution approach, the increased degrees of freedom of the VS will enhance the capability of an array to determine the properties of independent sources [6] or to produce brightness distribution images from direction-cosine (u,v) plane measurements (i.e. Fourier interferometric synthesis imaging). Initial work in this area includes that of [7] who discuss VS arrays in the context of linear nested arrays, the co-array formalism, and a tensor modelling approach. However, the three dimensional nature of imaging in space is challenging because there is no ground plane below the antenna array and non-coplanarity of the array must be carefully treated [4].

VSI provides significantly more information per baseline than systems that do not fully sample the information content of electromagnetic waves at each point in the array. This information is represented by the electromagnetic covariance matrix $C_f = \boldsymbol{\varepsilon}(\boldsymbol{\mathcal{F}}\boldsymbol{\mathcal{F}}^{\boldsymbol{T}})$ representing the mathematical expectation of the electromagnetic source vector over all sources and between all pairs of vector sensor antenna elements in an array, and computed from the low-level RF voltage data from the individual VS elements. The dimensionality of vector space C_f determines the number of basis vectors required to span the space. This in turn determines the maximum number of sources that can be distinguished or, equivalently, the number of independent parameters that can be estimated to form an image using a given model basis (such as Fourier (u,v) sampling or spherical harmonics) and a deconvolution approach.

The maximum number of sources that can be resolved from a single point in space using second order statistics is one less than the dimensionality. Since a VS provides the same dimensionality as free space, it is not possible to construct a sensor that outperforms a VS in this aspect. For example, the dimensionality of a single vector sensor is 20 [2] compared to 6 for a tripole antenna and 1 for a dipole. In general, arrays of vector sensors provide a much higher dimensionality for cases where the sources are not aligned degenerately relative to the array configuration. For example, interferometry with two VS has a dimensionality of 71, while a tripole pair has 21 and a dipole pair only has 3. The high dimensionality of the VS translates directly into the ability of a sparse interferometric imaging array to measure quantities of interest such as numbers of independent sources, parameters of the electromagnetic source, or coefficients of an imaging model. Additionally, unlike tripole and dipole antennas, the VS can determine information about the magnetic field that allows it to distinguish electrostatic from electromagnetic wave modes.

Finally, while the communication burden for each node is greater than that of a traditional antenna, the overall data volume from a VSI array is comparable to or less than that of a traditional array of similar capability. Currently this burden is tractable for constellations that handle moderate RF bandwidths, and can be accommodated with a limited number of ground stations.

VS Beamforming and Nulling of Interference

To increase sensitivity for weak or distant targets, beamforming is a baseline technique for array applications. Minimum noise variance beamforming using a VS is an attractive technique in this context. This approach has advantages that include beamforming in three-dimensional space, the ability to receive and reject signals based on both their polarization and direction of arrival (DOA), and the ability to handle more signals in beamforming applications compared to scalar array. The signal handling follows directly from the available dimensionality. Beamforming can be applied to a single VS, a VS sparse array, or to reduce the data from a VS to a single combined vector measurement prior to interferometry.

A useful performance metric for beamforming assessment is the signal to interference-plus-noise ratio (SINR) [8]. The VS provides a significant advantage in SINR for regions well-separated from the interfering source, or where the source and interferer polarizations differ significantly. These performance qualities have significant implications for radio remote sensing. Traditionally, the conventional assumption is that interference would preclude sensitive low frequency radio imaging in the near-Earth space environment. This has led mission designers to seek lunar far-side shielding, despite the multiple penalties of costly launches, low data rates, and need for in-space correlation. The high dimensionality of a VS array enables direct nulling of interfering sources and thus it can operate close to Earth, an extraordinary advantage compared to more traditional approaches.

FLIGHT SYSTEM

The VISTA CubeSat bus will be procured and integrated by Morehead State University (MSU). The VS payload will be developed by MIT Lincoln Laboratory (MIT-LL) and integrated by MIT Haystack Observatory (MIT-HO). AERO and VISTA will have identical functionality in hardware, firmware, and software.

Along-Track Positioning Using Drag

After being deployed together, the along-track AERO and VISTA separation will be controlled by differential drag (cross-track drift is typically negligible on the scale of several months). The drag force on a CubeSat is $\rho A v^2$, where the atmospheric gas density ρ is 3×10^{-12} kg/m^3 at 400 km altitude, A is the area presented to the direction of motion (~100 to ~ 300 cm^2 for VISTA), and v is the orbital velocity (~ 7 km/s). Time varying separation of a pair of identical CubeSats is given by the differential equation

$$\frac{d^2\Delta}{dt^2} = \frac{\rho\,(A_1 - A_2)v^2}{m} \qquad (2)$$

where m ~6 kg. Integration yields the time t required to reach a separation Δ:

$$t = \sqrt{\frac{2\Delta}{\alpha}}\;;\; \alpha \equiv \frac{\rho\,(A_1 - A_2)v^2}{m} \qquad (3)$$

For the maximal aspect difference (200 cm^2), α ~ 5 x 10^{-7} m/s^2. Thus, a week is required to achieve a separation of 100 km. If the CubeSats present roughly the same area to the direction of motion ($A_1 \approx A_2$), there is no tendency to separate to great distances along the orbital track. The only requirements placed on the VISTA and AERO are (1) that they be power positive with the required aspect and (2) that we have effective attitude control authority to be able to maintain the desired relative orientation for the time required. Differential drag orbit control has been demonstrated on-orbit. See [9], [10] for a description of differential drag control of the Planet 'flock'.

As a proof-of-concept, TLE-derived radial, along-track, cross-track, and range data for two 6U CubeSats (Dellingr [11] and EcAMSat [12]) are shown in Fig. 1. Starting ~100 km apart, they drift to ~400 km in 3 months and then drift back to near-zero separation. Cross-track separation, which differential drag cannot effectively control, remains below 10 km for over 6 months and is therefore not a concern for AERO and VISTA. The VS instrument is insensitive to orientation, so drag control maneuvers will not adversely affect science data collection.

Additional drag control analysis is underway using analysis tools developed for the CLICK mission [13], [14].

Operations

VISTA will be deployed alongside AERO in a low Earth orbit under the CubeSat Launch Initiative (CSLI) program. Following acquisition and initial checkout, a few days are required for VS calibration with known HF sources. After on-orbit checkout and calibration, VISTA and AERO will collect initial raw voltage measurements for use in interferometry experiments. An existing MIT Haystack controlled and licensed ground-based radio HF radio beacon just below the 20 meter band (15 MHz) will be used for interferometry experiments. Ground based vector sensor receivers in combination with ionospheric ray tracing may also be used to provide phase and amplitude closure quantities when observations are made above the ionospheric cutoff frequency.

VISTA will also collect data in combination with AERO as it passes through or near the auroral oval. Since the primary sensor is omnidirectional, attitude control and pointing are only required for solar cell charging, telemetry, and relative position management of the two spacecraft. Secondary observations outside the auroral zone will also be made to provide general characterization of the LF/MF environment, and opportunistic measurements may be scheduled to capture solar radio bursts.

Downlink of housekeeping and survey data including GPS positioning, followed by as much of the flagged science data as possible from spacecraft memory, is collected in multiple daily passes at the Mission Operations Center (MOC) at MSU using their 21 m Deep Space Network antenna and at MIT Haystack Observatory using the 18 m Westford radio telescope.

Following downlink, mission data is assessed for completeness, and rapidly formatted and processed through a data pipeline to produce low level data products as well as state of health summaries and memory management reports. These are transferred from the MOCs to the Science Operations Center (SOC) at MIT-HO. At the SOC, interferometric experimental intervals, environmental survey data, and sources of interest (SoI), including AKR, LF Hiss, Roar and MFB events, are identified from the schedule and summary spectrograms (Fig. 2, see also [15], [16]). Twice daily, the spacecraft will be commanded with priorities for downlinking raw data.

DATA COLLECTION

VISTA requires data collection in combination with AERO to meet the interferometric measurement goals of the mission. By itself, VISTA is a duplicate of AERO and will provide redundancy in meeting AERO data sufficiency goals for auroral science. Combined experiments with VISTA and AERO will place

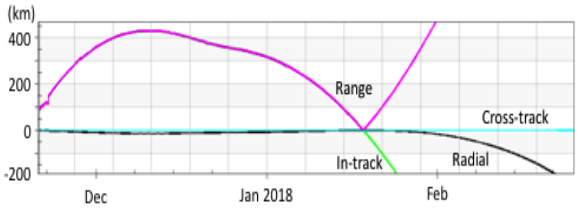

Figure 1: TLE-derived radial, along track, and cross-track distances for a pair of 6U CubeSats deployed from the International Space Station (ISS) several hours apart. Cross-track separation is <10 km for the first 6 months.

emphasis on collection of compressed raw voltage level data over limited bandwidths. This is already a planned operational mode for AERO but one which would otherwise be used primarily for calibration and signal processing validation activities. The collection of low level RF data from the two satellites will enable post-collection joint signal processing and analysis for interferometry and imaging using the two spacecraft and ground-based computing assets. Interferometric correlation will be performed on the ground.

A key technical demonstration of interferometry will use an existing MIT-HO controlled ground based radio source. VISTA will also be used with AERO to obtain selected intervals of compressed raw voltage level data for passes through the auroral zone. Contextual information from the onboard magnetometer and photometer will also be available to put each datum into an auroral context (e.g. Birkeland Region 1 auroral current region, visible aurora indicator, spacecraft location in magnetic coordinates using the International Geomagnetic Reference Field model (IGRF, [17]) and onboard magnetometer values).

VISTA survey modes will be operated identically to AERO and will provide 100 ms time resolution of

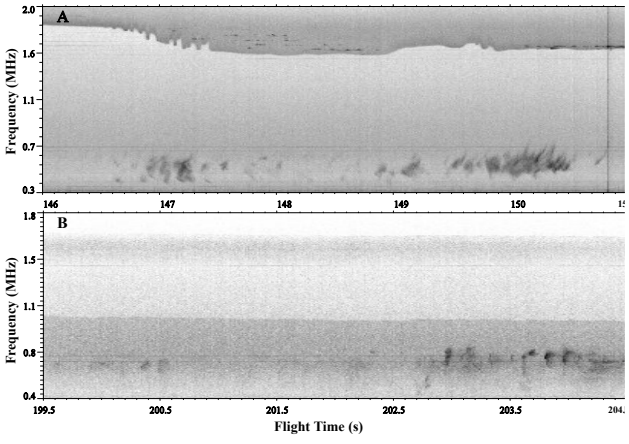

Figure 2: Radio spectrograms, typical of what AERO and VISTA may encounter.

survey spectrograms that are optimized for identification of known auroral radio emission types (auroral kilometric radiation (AKR), LF hiss, auroral roar, medium frequency burst (MFB)).

VISTA will use the MIT-HO Westford radio telescope (18 m) as a second ground station to allow for simultaneous downlink from the two spacecraft and coverage of a larger number of downlink opportunities. When events are identified, the covariance data will be downlinked from each spacecraft and evaluated. Following this, a decision will be made for combined VISTA and AERO observations selecting observations for downlink of raw data from the two spacecraft. The expected duration and frequency of four types of signals of interest are listed in Table 1. AKR and LF hiss are sufficiently strong that they can in nearly all cases be accessed with minimal integration. For MFB and some roar emissions, integration is likely required, but Table 1 indicates that in nearly all cases a 1 second integration is more than sufficient to enable detection.

To demonstrate VSI, Beamforming, and Nulling, we will collect compressed raw voltage data centered on the frequency of a ground based beacon located at MIT-HO for at least 100 s at 150 kHz bandwidth. Assuming 1:4 compression, each interval will require ~4 telemetry passes. To characterize the RFI environment in LEO, VISTA will collect both compressed raw data and survey plot information periodically over an orbit. Selected raw data intervals will be downlinked based on the content of the survey plots.

PAYLOAD

The vector sensor (VS) is composed of four subsystems: (1) the deployable antenna, (2) a multi-channel analog receiver, (3) a mixed-signal converter and on-orbit signal processor, and (4) payload memory and data management.

VS Antenna

The VS consists of 3 orthogonal dipoles and 3 electromagnetic loop antennas that, through signal processing, provide angle-of-arrival and polarization information for signals from 50 kHz to 20 MHz [18], [19]. AERO's science requirements imposed a 5 MHz usable upper frequency observation limit. In practice, however, the observable frequency range is implemented and selectable using a combination of sample clock rate and filtering. The ADC itself supports up to 80 MSPS on each receiver channel and thus will support a VISTA requirement of narrowband operation up to 15 MHz with an appropriate filter path and a programmable clock.

To meet launch constraints, the antennas will be deployed with fiberglass "tape measure" technology. VISTA has baselined 4-meter antennas (2 m in each direction), which are electrically short at the frequencies of interest, but are nevertheless sufficient to ensure that external electromagnetic signals dominate relative to internal noise. The antenna is extended in five directions from one end of the spacecraft and fits in 1U of payload space when stowed for launch [20], [21]. The loop antenna area is 0.8 m^2 for the crossed loops, and 8 m^2 for the perimeter loop. A recent design innovation unspools the antenna from fixed reference points within the payload body, simplifying the electrical connection and removing the need for slip rings. See Fig. 3 for payload design and antenna deployment sequence.

Table 1: Estimates of expected AERO / VISTA auroral emission duration, total bandwidth, amplitude, and event rates by emission type. Upper observation bound is set at 100- 300 s by spacecraft orbital motion.

Type	Duration (s)	Δf (kHz)	Intensity (W/m² Hz)	Rate (/day)
AKR	1 – 300	20 - 500	10^{-19}	0.2–0.33
LF Hiss	0.1 - 300	100 - 1000	10^{-19}–10^{-18}	0.33
MF Burst	0.1 - 300	100 - 3000	few 10^{-19} –>10^{-18}	0.1–0.3
Roar	0.1 - 300	50 - 200	few × 10^{-19} –> few x 10^{-18}	3
Beacon	1	1	> 10^{-15}	2 to 3 max

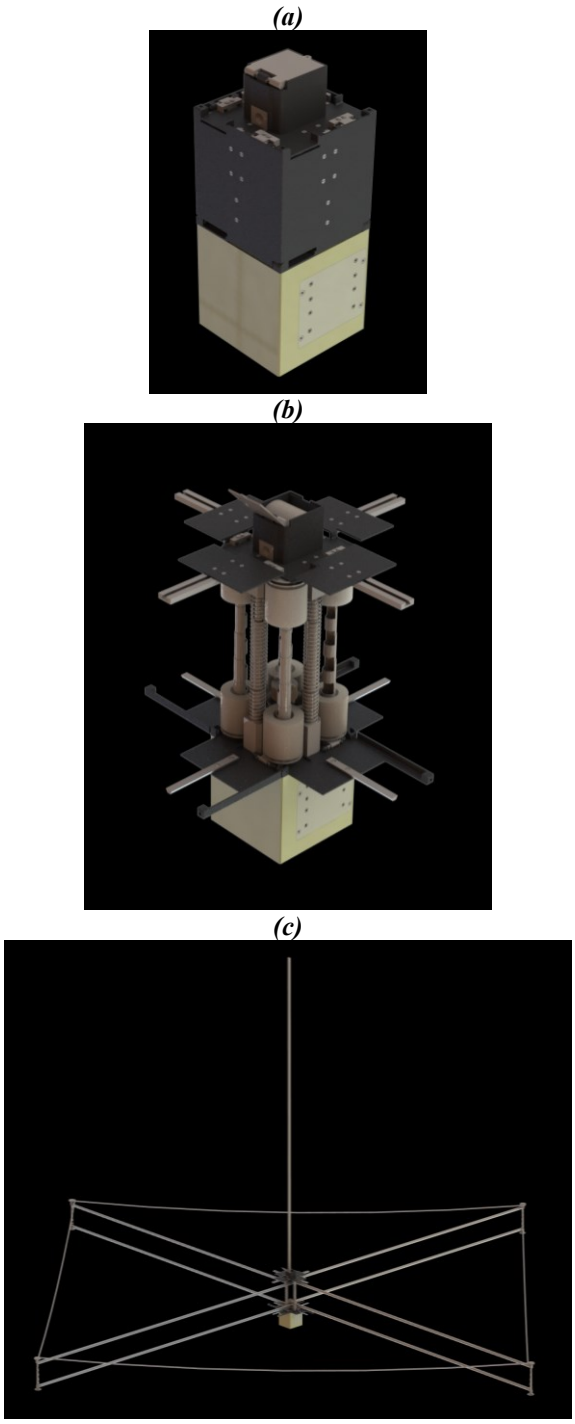

Figure 3. AERO/VISTA payload. The stowed payload (a) is composed of the antenna deployment canister (black) and the electronics box (gold). The system deploys in two stages. First, the top of the deployment canister expands upward (b). Then, the doors restraining the antenna open and the antenna unspools to its deployed configuration (c). The thickness of the perimeter loop is exaggerated for visibility.

Science receiver

The six-channel vector sensor radio receiver will be integrated into a stackup of two compact PC-104 form factor boards based on the CHREC CSP design using a larger version of the onboard Zynq FPGA. With its associated small backplane connector board, the receiver fits into 0.5U of payload space. The stackup consists of an analog front end board, followed by a mixed signal and Field-programmable gate array (FPGA) signal processor board. The receiver amplifies, filters, and converts the analog signals to digital by a direct RF sampling analog-to-digital converter (ADC). This is followed by initial digital signal processing in an FPGA processor.

The signal chain starts with a diode clipping circuit for protection against transients that result from, for example, micrometeoroid impacts. The antenna/receiver combination is made broadband using a high dynamic range charge pre-amplifier [22] that keeps the antenna-receiver referred noise level under 2nV/√Hz. The effective electrical length of 4 m antenna elements is 2 m, thus providing a free-space input-referred system noise floor of less than 1 nV/m/√Hz. The loop antennas are matched to the receiver by using the dual of the charge amplifier, that is, a transconductance amplifier, which also flattens the response across frequency. The sensitivity of two of the loops' antenna/receiver channels is approximately 5 dB less than the dipole antennas, but the sensitivity of the larger "perimeter loop" is comparable to the dipoles.

After the first stage of amplification there is a noise whitening stage that reduces dynamic range requirements of the ADC to accommodate the wide variation in expected external noise levels as a function of frequency. These antenna/receiver combinations provide the sensitivity required to meet the science objectives with minimal integration times (e.g. AKR), making them suitable for capturing transient events. A reference source will be injected into the front end to provide accurate absolute reference for sensitivity verification, channel-to-channel matching, and gain calibration.

Mixed signal converter

The six channels of analog receiver information are converted to digital in the first stage of the mixed signal converter and on-orbit signal processor board. The ADC conversion occurs at a maximum rate of 80 MHz using 16-bit converters with 93 dB spur-free-dynamic range. VISTA will use a programmable sample clock generator. We currently plan to run the ADCs at a rate of 51.2 MSPS with a maximum analog frequency of 15 MHz. The oversampling simplifies the analog low-pass

filter hardware requirements. The on-orbit signal processing will allow data to be collected and downlinked at either ADC sample rates or with a reduced, programmable frequency resolution. The sample clock will be derived from a Microsemi Space Qualified Chip Scale Atomic Clock reference signal using a phase locked loop. The CSAC can be selectively disciplined using the GPS PPS signal as a configuration parameter. The use of the Space CSAC will ensure sufficient clock stability to perform coherent interferometric measurements at the low frequencies of operation over all relevant time scales (e.g. seconds to minutes).

Data from the ADCs are streamed into an FPGA-based signal processor, based on the original CHREC CSP design modified to include a new Xilinx Zynq family chip, which has been prototyped and is currently being laboratory tested. The ADCs were incorporated onto the CHREC-format board by removing the redundant power supply area reserved for the non-space grade circuitry.

Memory and data management

Data from the VS and ASP are time-tagged with microsecond accuracy from the ADC sampling clock and the GPS pulse per second signal, then stored in payload memory. This memory is a solid state M.2 disk mounted on the CHREC form factor board in the payload backplane. Software on the Zynq signal processor board will be used to manage the data recording, format summary data for downlink, and respond to requests for data snapshots. Dual M.2 drives are designed into the payload for redundancy with only a single drive powered on at any time.

The 2 TB total payload memory will contain instrument data. These include compressed raw samples from the six elements, 100 ms resolution summary spectral data, and relevant metadata (timing, attitude, orbital parameters, DC-magnetic field orientation in the spacecraft frame and coarse photometry to detect optical auroral emission), as well as covariance information computed from the 6 signals (3-axis E and 3-axis B) and averaged over 100 msec time resolution. The summary data will be automatically downlinked to support science team selection of signals of interest. Data products that are requested from the ground are protected from being overwritten in the circular buffer and are prioritized for downlink. Data from other time-segments retain their default priority and are eventually overwritten based on their age. High-resolution covariance data will be compressed channel-by-channel so that the available storage is adequate to support an operational daily cadence of event selection and downlink. Raw data segment retention will be carefully planned and retain limited RF bandwidths (e.g. 150 kHz). The payload memory board also includes the power supply conditioning and monitoring circuitry for the payload.

RADIATION, EMI AND EMC

The VS is built primarily from industrial grade parts with judicious use of space-rated parts to mitigate risk of destructive single event upset or reduced lifetime in a manner consistent with 3 months of operations on orbit. Single-event-upset circuitry developed for another space project is incorporated into the radio. Since the Zynq and solid state disks are not space-rated parts, recovery from single event upsets will be accomplished by power cycling. We will use a high reliability space qualified micro-controller to monitor the power supply rails for unexpected surges and to respond to a periodic watchdog signal. Failure to meet the watchdog interval or exceeding a programmable timeout will result in an automatic power cycling of the payload.

Both VISTA and AERO require that there be no significant signal degradation from the commercial off-the-shelf quality bus or other subsystems that might couple or radiate into the receiver or antenna. Conducted and radiated self-interference will be managed by the following methods:

- Electrostatic shielding of the bus components and the receiver.
- Power supply filtering in the payload memory board and radiation suppression through the use of ferrite beads.
- Suppression of emission from power lines and solar panels by shielding and ferrites.
- Characterization of remaining spurs, such as discrete radiated emissions from power supplies. As long as less than 1% of the polyphase filter bank frequencies are not impacted then there will be little impact to the overall science mission.

SIGNAL PROCESSING

The digital signal processing includes a polyphase filterbank to channelize the signals in frequency and to create “waterfall” spectrogram plots that can be used to isolate signals of interest. Raw data, partially processed or compressed for compactness is written to non-volatile memory for further processing and/or selective downlink.

For interferometry measurements, the compressed raw data is needed from both AERO and VISTA for a simultaneous interval. For other cases, the intensity,

direction of arrival and polarization state of science sources are contained in a data covariance matrix, which captures the intensity and relationship of the signals received between each of the antenna elements. Further, the Hermitian-symmetric covariance matrix has a unique Cholesky upper/lower triangular decomposition, which is a more compact representation that also requires half the number of bits as the covariance [23]–[27]. The Cholesky factor is directly computed from the raw data through a process referred to as a QR decomposition [28]–[30]. A block form of the Cholesky can be computed for the two-spacecraft interferometer using a mixture of individual spacecraft Cholesky factors and time series corresponding to the signal subspace from each spacecraft.

The FPGA processor will perform the QR decomposition in each polyphase filter channel prior to storage. Since data acquisition is only required over selected regions (e.g. an auroral oval), the processing for the Cholesky factorization from a temporary data cache is nominally scheduled for portions of the orbit that are outside of the observation and telemetry windows.

AUXILIARY SENSOR PACKAGE

The Auxiliary Science Package (ASP) provides photometry, for independent confirmation of auroral events, and a magnetometer, to localize VISTA / AERO observations with respect to the auroral oval through observations of Birkeland Region 1 currents.

Photometry measurements are made by a single chip photometer/spectrometer with six spectral bands. The available spectral channels cover both auroral red line (630 nm) and green line (557.7 nm) emission. Only one sensor is required for auroral arc context measurements, though three are included in the current design for redundancy and operational flexibility.

AERO has baselined the PNI RM3100 magnetometer for magnetic field context measurements. The ASP will include 2-4 magnetometers in different physical locations within the payload. The placement and calibration approach will follow that of Regoli et al. (2018) [31]. Based on the results presented in [31], this system is expected to exceed the required magnetic field amplitude precision of 100 nT, which is needed to detect Birkeland Region 1 currents.

CALIBRATION

The Pattern Response Equalization for Spatial Symmetry (PRESS) algorithm is a maximum-likelihood technique for determining sensor calibration, and is our proven approach to determining element gain and pattern responses [32], [33]. This allows the VS calibration to factor in mutual coupling that is likely to be induced due to, for example, the solar panels and antenna elements. Accuracy of the vector sensor on a replica unmanned air vehicle (UAV) using PRESS was reported in [32].

MIT-LL will calibrate the VS spatial angles, signal frequency, gain from free-space to digital data, amplitude, polarization, and frequency of the individual antennas. Receiver noise floor and dynamic range will be ground-tested in the MIT-LL System Test Chamber, which as a Faraday cage provides >20 dB inherent shielding from external sources in the LF/MF frequency range [34]. The antenna element pattern and the effective height and loss of the electrically small loops and dipole responses will be measured in the MIT-LL RF Systems Test Facility. In flight, a stable NIST-traceable noise diode or comb generator, depending on the specific calibration, will be injected into the six antenna inputs to determine channel-to-channel gain and phase differences as well as the absolute gain of the receiver system. The VS antenna element gains as a function of angle will be measured by rotation of the spacecraft while observing the ground-based beacon.

DATA ANALYSIS METHODOLOGY

VISTA telemetry consists of summary spectrogram plots, data products for selected signals of interest, attitude information from the star trackers, and housekeeping data. The VS provides 3-axis E and B signals in the spacecraft frame with both compressed raw voltage and covariance data available for downlink. At LEO altitudes, the IGRF model [17] is adequate to rotate into geomagnetic coordinates; the flight magnetometer provides a consistency check and will track magnetospheric distortions during active periods. The magnetometer is used to estimate auroral zone field-aligned Birkeland currents. Photometry from the spectrometer will identify significant optical emissions.

Data is stored on the spacecraft in the form of compressed raw voltages, Cholesky factorization of the sample covariance in block floating point format, one fixed-point mantissa per element and a single multiplier for the block. The Cholesky factors provide access to the electromagnetic character of the radio signals detected on orbit and allow determination of the Poynting vector. In conjunction with a model magnetosphere and an estimate of plasma density (from resonance cutoffs), observed auroral radio emission will be ray-traced to probable source regions.

SUMMARY

The Vector Interferometry Space Technology using AERO mission (VISTA), will complement the Auroral Emission Radio Observer (AERO) with a build-to-print companion spacecraft.

Together, VISTA and AERO will provide the first space demonstration of interferometric imaging, beamforming, and nulling using electromagnetic vector sensors (VS). This combined mission will demonstrate that VS interferometry can enable significantly smaller radio sensing constellations that maintain sensitivity even in the presence of substantial terrestrial interference.

By dramatically improving angular resolution, the twin AERO and VISTA spacecraft will open a broad Discovery Space for spatially and temporally complex auroral and solar phenomena. VISTA will also expand the scientific return and robustness of the AERO investigation by significantly increasing the quantity and breadth of observations and providing redundancy.

Acknowledgments

The VISTA project is supported by NASA opportunity NNH18ZDA001N-HTIDS in the Heliophysics Heliophysics Technology and Instrument Development for Science program. The AERO project is supported by NASA opportunity NNH17ZDA001N-HTIDS in the Heliophysics Heliophysics Technology and Instrument Development for Science program. Any opinions, findings, conclusions or recommendations expressed in this material are those of the author(s) and do not necessarily reflect the views of NASA.

References

[1] P. Erickson *et al.*, "AERO: Auroral Emissions Radio Observer," in *32nd Annual AIAA/USU Conference on Small Satellites*, 2018.

[2] M. Knapp *et al.*, "Vector Antenna and Maximum Likelihood Imaging for Radio Astronomy," in *IEEE Aerospace*, 2016.

[3] I. H. Cairns, S. A. Knock, P. A. Robinson, and Z. Kuncic, "Type II Solar Radio Bursts: Theory and Space Weather Implications," in *Advances in Space Environment Research - Volume I*, Dordrecht: Springer Netherlands, 2003, pp. 27–34.

[4] T. J. Cornwell, "Radio-interferometric imaging of very large objects," *Astron. Astrophys.*, vol. 202, pp. 316–321, 1988.

[5] J. P. Hamaker, J. D. Bregman, and R. J. Sault, " Understanding radio polarimetry. I. Mathematical foundations ," *Astron. Astrophys. Suppl. Ser.*, vol. 117, no. 1, pp. 137–147, 1996.

[6] R. Volz, M. Knapp, F. Lind, and F. Robey, "Covariance Estimation in Terms of Stokes Parameters with Application to Vector Sensor Imaging," in *50th Asilomar Conference on Signals, Systems and Computers*, 2016.

[7] K. Han and A. Nehorai, "Nested vector-sensor array processing via tensor modeling," *IEEE Trans. Signal Process.*, vol. 62, no. 10, pp. 2542–2553, 2014.

[8] A. Nehorai, K. C. Ho, and B. T. G. Tan, "Minimum-noise-variance beamformer with an electromagnetic vector sensor," *IEEE Trans. Signal Process.*, vol. 47, no. 3, pp. 601–618, 1999.

[9] C. Foster, H. Hallam, and J. Mason, "Orbit determination and differential-drag control of Planet Labs cubesat constellations," in *Advances in the Astronautical Sciences*, 2016, vol. 156, pp. 645–657.

[10] C. Foster *et al.*, "Constellation Phasing with Differential Drag on Planet Labs Satellites," *J. Spacecr. Rockets*, vol. 55, no. 2, pp. 473–483, Mar. 2018.

[11] C. Clagett *et al.*, "Dellingr: NASA Goddard Space Flight Center's First 6U Spacecraft," *AIAA/USU Conf. Small Satell.*, Aug. 2017.

[12] A. C. Matin *et al.*, "EcAMSat: Effect of Space-Flight on Antibiotic Resistance of a Pathogenic Bacterium and its Genetic Basis," Nov. 2015.

[13] D. J. Mayer, J. L. Fishman, and K. Cahoy, "CubeSat Laser Infrared CrosslinK," Apr. 2019.

[14] D. J. Mayer, J. L. Fishman, and B. Schweighart, "CubeSat Laser Infrared CrosslinK (CLICK): A Demonstration of Flexible High-Data-Rate, Low-Cost, Full-Duplex CubeSat Optical Communications and Ranging Capability," Apr. 2019.

[15] N. Shutte, I. Prutensky, S. Pulinets, Z. Kłos, and H. Rothkaehl, "The charged-particle fluxes at auroral and polar latitudes and related low-frequency auroral kilometric radiation-type and high-frequency wideband emission," *J. Geophys. Res. A Sp. Phys.*, vol. 102, no. A2, pp. 2105–2114, 1997.

[16] J. LaBelle, K. L. McAdams, and M. L. Trimpi, "High-frequency and time resolution rocket observations of structured low- and medium-frequency whistler mode emissions in the auroral ionosphere," *J. Geophys. Res. Sp. Phys.*, vol. 104, no. A12, pp. 28101–28107, Dec. 1999.

[17] E. Thébault *et al.*, "International geomagnetic reference field: The 12th generation international geomagnetic reference field - The

twelfth generation," *Earth, Planets Sp.*, vol. 67, no. 1, p. 79, Dec. 2015.

[18] F. C. Robey, "High Frequency Geolocation and System Characterization (HFGeo) Phase 1B Proposers' Day Briefing: HFGeo Phase 0 and Phase 1B Test and Evaluation," 2012. [Online]. Available: http://www.iarpa.gov/images/files/programs/hfgeo/120710_Phase1B_Proposers_Day_Part2.pdf.

[19] M. Knapp *et al.*, "Vector antenna and maximum likelihood imaging for radio astronomy," in *IEEE Aerospace Conference Proceedings*, 2016, vol. 2016-June.

[20] F. C. Robey *et al.*, "High Frequency (HF) Radio Astronomy from a Small Satellite," in *30th Annual AIAA/USU Conference on Small Satellites*, 2016.

[21] M. Knapp *et al.*, "HF Vector Sensor for Radio Astronomy: Ground Testing Results," in *AIAA SPACE 2016*, 2016.

[22] R. N. Grubb, R. C. Livingston, and T. W. Bullett, "A new general purpose high performance HF Radar.," *URSI Gen. Assemby*, pp. 1–8, 2008.

[23] J. D. Tebbens and M. Tuma, "Matrix Inversion and Condition Estimation with Triangular Factors," in *Joint French-Czech Workshop on Krylov Methods for Inverse Problems*, 2010.

[24] A. Kielbasifrski, "A Note on Rounding-Error Analysis of Cholesky Factorization."

[25] J. Demmel, "On Floating Point Errors in Cholesky," in *LAPACK Working Note 14*, 1989.

[26] J. H. Wilkinson, "A priori error analysis of algebraic processes," in *Proceedings of the International Congress of Mathematicians, 1966*, 1968, pp. 629–640.

[27] L. Vandenberghe, "EE133A Lecture Notes, spring quarter 2017." [Online]. Available: http://www.seas.ucla.edu/~vandenbe/133A/133A-notes.pdf.

[28] L. Miller, "Adaptive Beamforming for Radar : Floating-Point QRD + WBS in an FPGA," 2014.

[29] G. H. Golub and C. F. Van Loan, *Matrix computations*. 1996.

[30] H. L. Van Trees, *Detection, estimation, and modulation theory. [Part III], Radar-sonar signal processing and Gaussian signals in noise*. Wiley, 2001.

[31] L. H. Regoli, M. B. Moldwin, J. Thoma, M. Pellioni, and B. Bronner, "Four-Magnetometer Board for CubeSat Applications," in *32nd Annual AIAA/USU Conference on Small Satellites*, 2018.

[32] S. Appadwedula and C. M. Keller, "Direction-Finding Results for a Vector Sensor Antenna on a Small UAV," in *Fourth IEEE Workshop on Sensor Array and Multichannel Processing, 2006.*, 2006, pp. 74–78.

[33] L. L. Horowitz, "Airborne Signal Intercept for Wide-Area Battlefield Surveillance," *LINCOLN Lab. J.*, vol. 10, no. 2, 1997.

[34] A. J. Fenn, M. W. Shields, and G. A. Somers, "Introduction to the New MIT Lincoln Laboratory Suite of Ranges," in *26th Annual Antenna Measurement Techniques Association Meeting & Symposium, AMTA*, 2004.